The 2010 IEEE/RSJ International Conference on
Intelligent Robots and Systems
October 18-22, 2010, Taipei, Taiwan

Momentum Conserving Path Tracking Through Dynamic Singularities With a Flexible-Base Redundant Manipulator

Naoyuki Hara[1], Dragomir Nenchev[2], Qiao Sun[3] and Daisuke Sato[2]

Abstract— **High-speed path tracking with a kinematically redundant manipulator mounted on a flexible base is addressed. Thereby, possible vibrations of the base are to be suppressed. In general, the presence of kinematic redundancy allows these two subtasks to be performed simultaneously. In practice, however, this can be done only within very limited areas of workspace, separated by singularity loci that change dynamically while the end-effector tracks the desired path. To avoid controller performance degradation in the neighborhood of such dynamic singularities, and to allow transitions between the distinct workspace areas through singularity boundaries, we propose here a new method for reactionless motion generation within a specified neighborhood of the singularity. In contrast to previous works, this method makes use of a nonzero coupling momentum which is conserved upon entering the neighborhood.**

I. INTRODUCTION

Flexible-base robots have been studied widely in the past addressing such application fields as nuclear waste cleanup [1], [2] and space robotics [3], [4]. In the former application, a manipulator is mounted on a long beam to ensure access to a remote site. In the latter application, the manipulator is mounted at the end of a large arm that allows relocation of the manipulator base. Such systems are known as "macro-micro" manipulators. Examples include the Canadian SSRMS/Dextre and the Japanese JEMRMS/SFA manipulator systems on the International Space Station. It is worth noting that flexible-base robot control methods are being studied also within the fields of industrial robotics [5] and humanoid robotics [6], [7].

Flexible-base robots represent a challenge from the control point of view. The reason is the dynamic coupling between the motion of the manipulator(s) and that of the flexible base. Vibrations can be induced into the base by a disturbance wrench imposed via manipulator link motion. These vibrations deteriorate performance and even may destabilize the system. Numerous studies on the problem exist already. Some deal with pure vibration suppression via inertial damping [8]–[12], others propose command generation for minimizing base disturbance [13] or tackle the problem of end-link control in the presence of vibrations [14], [15].

In this work we consider a subclass of flexible-base robots that are required to track a desired path with their end-effectors. One possible approach to avoid base disturbance thereby is reactionless motion generation and control. As shown in [16], this can be achieved by employing the Reaction Null-Space method developed initially for free-floating space robots [17]. It turned out, however, that the constraint imposed via the Reaction Null-Space leads to a restricted workspace [18], [19]. To alleviate the problem, in [18] we examined trajectory tracking performance under vibration suppression control only. Though the method allows the base to deflect, consequent base vibrations are successfully suppressed.

Note on the other hand, that the imposed vibration suppression constraint leads to the appearance of *dynamic singularities*, first noticed in a study on free-floating space robots [20]. Under conventional control, stability cannot be guaranteed anymore upon entering a specified neighborhood of such singularities. Various methods, notably *singularity avoidance* path planning strategies, have been developed so far to deal with singularities, but most frequently the better understood kinematic singularities were addressed. Singularity avoidance, however, is not applicable in the case of dynamic singularities located within the workspace. In contrast to kinematic singularities, the loci of dynamic singularities change with the variation of the arm configuration thus rendering path planning for singularity avoidance a very difficult problem. This is the reason why we preferred a *motion-through-singularity* strategy in [21]. To avoid destabilization, the vibration suppression capability was simply switched off upon entering a specified vicinity of the dynamic singularity. In this way, we could ensure stability, but nevertheless, the lack of vibration suppression control in the neighborhood lead to undesirable base deflection and non-smooth trajectories, especially for higher tracking speeds.

The aim of the present work is to improve *path tracking* performance along paths that cross dynamic singularities with a relatively high tracking speed. Thereby, the flexible base should not be significantly disturbed and stability should not be compromised as well. We will show that this problem can be tackled via coupling momentum conservation while crossing the dynamic singularity. This means reactionless motion generation under nonzero initial conditions.

The paper is organized as follows. In Section II, we present background and notations. In Section III, we introduce a path tracking control method with momentum conservation under nonzero initial condition. In Section IV, we discuss path tracking and control with a planar 3R flexible-base redundant manipulator as a case study. The conclusions are given in Section V.

N. Hara, D. Nenchev and D. Sato are with Tokyo City University, 1-28-1, Tamazutsumi, Setagaya-ku, Tokyo 158-8557, Japan.

Q. Sun is with the Department of Mechanical and Manufacturing Engineering, University of Calgary, Calgary, Alberta, Canada T2N 1N4.

[1] hara@rls.mse.tcu.ac.jp
[2] {nenchev, dsato}@tcu.ac.jp
[3] qsun@ucalgary.ca

II. BACKGROUND AND NOTATIONS

In this paper, we employ a model-based approach to design a suitable controller under the idealized assumption of perfect model match. Issues related to model uncertainty and robustness are out of the scope of the present work.

A. Equation of motion

The equation of motion of a flexible-base manipulator can be written in the following form [16]:

$$\begin{bmatrix} \boldsymbol{H}_b & \boldsymbol{H}_{bm} \\ \boldsymbol{H}_{bm}^T & \boldsymbol{H}_m \end{bmatrix} \begin{bmatrix} \dot{\mathcal{V}}_b \\ \ddot{\boldsymbol{q}} \end{bmatrix} + \begin{bmatrix} \boldsymbol{c}_b \\ \boldsymbol{c}_m \end{bmatrix} + \begin{bmatrix} \boldsymbol{D}_b \mathcal{V}_b \\ \boldsymbol{D}_m \dot{\boldsymbol{q}} \end{bmatrix} + \begin{bmatrix} \boldsymbol{K}_b \Delta\mathcal{X}_b \\ \boldsymbol{0} \end{bmatrix} = \begin{bmatrix} \boldsymbol{0} \\ \boldsymbol{\tau} \end{bmatrix}, \quad (1)$$

where subscripts $(\circ)_m$ and $(\circ)_b$, stand for manipulator and base, respectively. Caligraphic characters denote spatial vector quantities, e.g. the spatial (position/orientation) deflection of the base from its equilibrium $\Delta\mathcal{X}_b \in \Re^k$ and the twist (spatial velocity) $\mathcal{V}_b \in \Re^k$. $\boldsymbol{q} \in \Re^n$ stands for the generalized coordinates of the manipulator, $\boldsymbol{H}_b$, $\boldsymbol{D}_b$, and $\boldsymbol{K}_b \in \Re^{k\times k}$ denote base inertia, viscous damping and stiffness, respectively. $\boldsymbol{H}_m(\boldsymbol{q}) \in \Re^{n\times n}$ is the inertia matrix of the manipulator, $\boldsymbol{D}_m$ stands for joint viscous damping. Matrix $\boldsymbol{H}_{bm}(\Delta\mathcal{X}_b, \boldsymbol{q}) \in \Re^{k\times n}$ denotes the so-called inertia coupling matrix. $\boldsymbol{c}_b(\Delta\mathcal{X}_b, \boldsymbol{q}, \mathcal{V}_b, \dot{\boldsymbol{q}})$ and $\boldsymbol{c}_m(\Delta\mathcal{X}_b, \boldsymbol{q}, \mathcal{V}_b, \dot{\boldsymbol{q}})$ are velocity-dependent nonlinear terms, and $\boldsymbol{\tau} \in \Re^n$ is joint torque. No external forces are acting neither on the base nor on the manipulator.

B. Dual task formulation and dynamic singularities

We aim to simultaneously control both end-effector motion and base reaction. Consider first the motion of the flexible base. The base dynamics, derived from the equation of motion (1), can be written as:

$$\boldsymbol{H}_b \dot{\mathcal{V}}_b + \boldsymbol{D}_b \mathcal{V}_b + \boldsymbol{K}_b \Delta\mathcal{X}_b = \mathcal{W}_b, \quad (2)$$

where the quantity on the r.h.s. is the *base reaction wrench* that appears in response to the wrench imposed on the base by manipulator motion:

$$\mathcal{W}_m = -\mathcal{W}_b = \boldsymbol{H}_{bm}\ddot{\boldsymbol{q}} + \dot{\boldsymbol{H}}_{bm}\dot{\boldsymbol{q}}. \quad (3)$$

$\mathcal{W}_m$ will be henceforth referred to as the *imposed wrench*. Hereby, it was assumed that the base deflection is small, and also that $\boldsymbol{c}_b \approx \dot{\boldsymbol{H}}_{bm}\dot{\boldsymbol{q}}$. The imposed wrench can be also represented as the time derivative of the *coupling momenta*:

$$\mathcal{L}_m = \begin{bmatrix} m_{tot}\dot{\boldsymbol{r}}_c \\ \boldsymbol{r}_c \times m_{tot}\dot{\boldsymbol{r}}_c + \sum_{j=1}^{n} (\boldsymbol{I}_j\boldsymbol{\omega}_j + \boldsymbol{r}_j \times m_j\dot{\boldsymbol{r}}_j) \end{bmatrix}, \quad (4)$$

where $\boldsymbol{r}_c$ stands for the position of the total CoM of the manipulator, $\boldsymbol{I}_j$, $\boldsymbol{\omega}_j$, m_j, $\boldsymbol{r}_j$ stand for the inertia matrix, angular velocity, mass and CoM position for link j, respectively, and m_{tot} is the total mass of the manipulator.

Next, denote by $\mathcal{V}_e = \begin{bmatrix} \boldsymbol{v}_e^T & \boldsymbol{\omega}_e^T \end{bmatrix}^T \in \Re^m$ the end-effector twist. Its rate can be written as:

$$\dot{\mathcal{V}}_e = \boldsymbol{J}_e\ddot{\boldsymbol{q}} + \dot{\boldsymbol{J}}_e\dot{\boldsymbol{q}} + \dot{\mathcal{V}}_b, \quad (5)$$

where $\boldsymbol{J}_e(\boldsymbol{q}) \in \Re^{m\times n}$ is the end-effector Jacobian. Combining the imposed base motion constraint (3) with the above end-effector acceleration constraint, we obtain:

$$\begin{bmatrix} \dot{\mathcal{V}}_e \\ \mathcal{W}_m \end{bmatrix} = \boldsymbol{A}\ddot{\boldsymbol{q}} + \dot{\boldsymbol{A}}\dot{\boldsymbol{q}} + \begin{bmatrix} \dot{\mathcal{V}}_b \\ \boldsymbol{0} \end{bmatrix}, \quad (6)$$

where $\boldsymbol{A} = \begin{bmatrix} \boldsymbol{J}_e^T & \boldsymbol{H}_{bm}^T \end{bmatrix}^T \in \Re^{(m+k)\times n}$. Assume $m + k \leq n$. The joint acceleration can be then written as:

$$\ddot{\boldsymbol{q}} = \boldsymbol{A}^+ \left(\begin{bmatrix} \dot{\mathcal{V}}_e \\ \mathcal{W}_m \end{bmatrix} - \dot{\boldsymbol{A}}\dot{\boldsymbol{q}} - \begin{bmatrix} \dot{\mathcal{V}}_b \\ \boldsymbol{0} \end{bmatrix} \right) + \boldsymbol{n}_A, \quad (7)$$

where $(\circ)^+$ denotes a pseudoinverse. $\boldsymbol{n}_A$ denotes a vector from the kernel of $\boldsymbol{A}$, which is null when there are no redundant DOFs ($m + k = n$).

It should be clear that if a control law is based on the above joint acceleration, in the neighborhood of singularities of $\boldsymbol{A}$, where $\det(\boldsymbol{A}\boldsymbol{A}^T) = 0$, performance will inevitably degrade and the system may destabilize. These singularities include the subset of kinematic singularities defined by the condition $\det(\boldsymbol{J}_e\boldsymbol{J}_e^T) = 0$. Other singularity subsets are of dynamic nature and are located within the workspace. The loci of these singularities change continuously as a function of the manipulator configuration. We will refer to these latter singularities as *dynamic singularities*.

In an attempt to tackle path tracking control in the presence of dynamic singularities, we resolved (6) as [21]:

$$\ddot{\boldsymbol{q}} = \boldsymbol{J}_e^+ \left(\dot{\mathcal{V}}_e - \dot{\boldsymbol{J}}_e\dot{\boldsymbol{q}} - \dot{\mathcal{V}}_b \right) + \boldsymbol{n}_{J_e}(\mathcal{W}_m), \quad (8)$$

where $\boldsymbol{n}_{J_e}(\mathcal{W}_m)$ is the subset of vectors in the kernel of the manipulator Jacobian that dependent upon the imposed wrench. We used this notation for vibration suppression, injecting thereby additional (inertial) damping into the base dynamics via the relation $\mathcal{W}_b = -\mathcal{W}_m = -\boldsymbol{G}\mathcal{V}_b$, $\boldsymbol{G}$ denoting a positive definite matrix for spatial damping. Of course, the dynamic singularities did not disappear, but it became possible to devise a computed torque control law for avoiding destabilization during path tracking, by simply removing the null space component in the last equation while crossing the singularity.

III. MOMENTUM CONSERVATION BASED PATH TRACKING CONTROL

While we succeeded in avoiding destabilization while crossing a dynamic singularity, it became apparent that the base will be disturbed by the induced reaction [21]. The magnitude of base disturbance depends on the rate of the momenta $\mathcal{L}_m$. Hence, to avoid such disturbance, the rate should be minimized. This suggests a momentum conservation strategy. Such a strategy can be easily achieved by inserting a zero base wrench in (7) and (8). Thus, upon entering a suitably defined neighborhood of the singularity, the secondary task in (8) is switched from vibration suppression ($\mathcal{W}_m = \boldsymbol{G}\mathcal{V}_b$) to momentum conservation ($\mathcal{W}_m = \frac{d}{dt}\mathcal{L}_m = \boldsymbol{0} \Rightarrow \mathcal{L}_m = \textbf{const}$). When leaving the neighborhood after crossing the singularity, the secondary task is switched back from momentum conservation to vibration suppression.

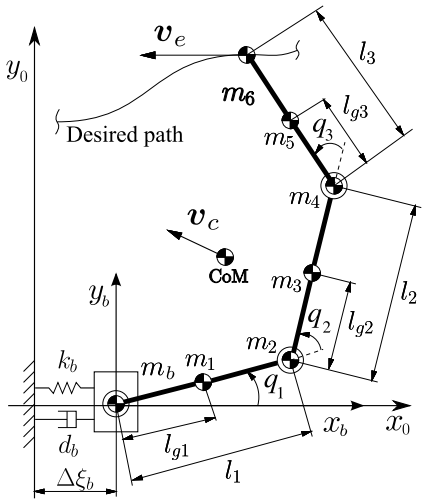

Fig. 1. Model of a planar three-link manipulator on a flexible base.

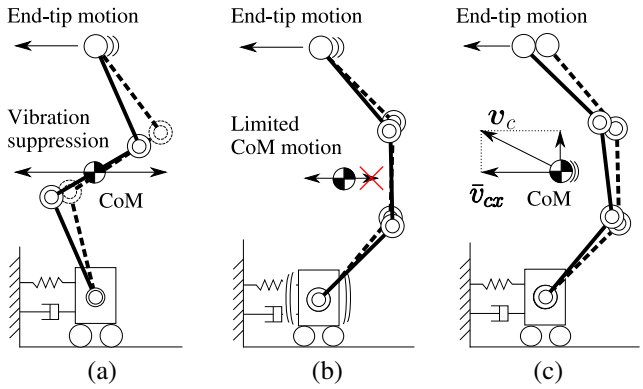

Fig. 2. Subtask performance capability: (a) simultaneous *trajectory tracking* and vibration suppression is possible away from a singularity; (b) in the neighborhood of a dynamic singularity, vibration suppression is impossible due to an unilateral constraint on the CoM motion; (c) in the neighborhood of a dynamic singularity, simultaneous *path tracking* and momentum conservation is possible.

Based on these relations, a computed torque dynamic controller can be designed with the reference joint acceleration:

$$\ddot{\boldsymbol{q}}^r = \boldsymbol{J}_e^+ \left(\dot{\mathcal{V}}_e^r - \dot{\boldsymbol{J}}_e \dot{\boldsymbol{q}} - \dot{\mathcal{V}}_b \right) + \boldsymbol{n}_{J_e}(\mathcal{W}_m^r), \tag{9}$$

where

$$\dot{\mathcal{V}}_e^r = \dot{\mathcal{V}}_e^d + \boldsymbol{K}_d(\mathcal{V}_e^d - \mathcal{V}_e) + \boldsymbol{K}_p(\mathcal{X}_e^d - \mathcal{X}_e), \tag{10}$$

$$\mathcal{W}_m^r = \begin{cases} \boldsymbol{K}_m(\bar{\mathcal{L}}_m^d - \mathcal{L}_m) & \text{if } t_{in} \le t \le t_{out} \\ \boldsymbol{G}\mathcal{V}_b & \text{otherwise.} \end{cases} \tag{11}$$

$\mathcal{X}_e$ denotes spatial position of the end-link, $(\circ)^r$ and $(\circ)^d$ are reference and desired values, respectively, $\boldsymbol{K}_p$, $\boldsymbol{K}_d$ and $\boldsymbol{K}_m$ are positive definite diagonal feedback gain matrices. t_{in} and t_{out} denote time instances for entering and leaving the neighborhood of a singularity, respectively. The former is determined as the time instant at which a component of interest of spatial base acceleration exceeds a given threshold: $|\dot{\mathcal{V}}_{bi}| \ge a_{max}$; the latter is the time instant when the determinant exceeds another given threshold: $|\det(\boldsymbol{A}\boldsymbol{A}^T)| \ge d_{max}$, a_{max} and d_{max} denoting the two thresholds. It should be apparent that the reference $\mathcal{W}_m^r$ is switched from vibration suppression to momentum conservation mode and vice versa. Thereby, the desired *constant* momentum $\bar{\mathcal{L}}_m^d = \mathcal{L}_m(t_{in})$ is determined in a "sample-and-hold" manner[1].

Note that in the case $m+k = n$, the conserved momentum path tracking strategy thus described might not be achievable for any path tracking speed, due to the loss of DOF at the singularity. A possible way to alleviate this problem will be described below with the following case study.

IV. CASE STUDY: 3R PLANAR MANIPULATOR ON A TRANSLATING FLEXIBLE BASE

Let us consider a 3R planar manipulator on a flexible base deflecting in the x direction while the end-tip tracks a specified path (Fig. 1). Since the manipulator has three DOFs ($n = 3$), it should be clear that outside the singularity neighborhood both the end-tip *trajectory tracking* ($m = 2$) and the vibration suppression ($k = 1$) subtasks can be performed simultaneously (Fig. 2 (a)). Upon entering the neighborhood, the motion of the manipulator CoM is restricted unilaterally as shown in Fig. 2 (b), and the vibration suppression capability deteriorates. Assuming that base deflection is negligible before entering the neighborhood, momentum can be conserved (the CoM moves with a constant-speed component $\bar{v}_{cx}$ as shown in Fig. 2 (c)) to ensure minimum base disturbance while crossing the singularity.

The driving torque needed to realize such a motion strategy is obtained from (1) as:

$$\boldsymbol{\tau} = \boldsymbol{H}_m \ddot{\boldsymbol{q}}^r + \boldsymbol{h}_{bm}^T \dot{v}_{bx} + \boldsymbol{D}_m \dot{\boldsymbol{q}} + \boldsymbol{c}_m, \tag{12}$$

where $\boldsymbol{h}_{bm} \in \Re^{1\times 3}$ stands for the coupling inertia row-vector. Since the system is planar, we will change henceforth the notation: $\mathcal{X} \to \boldsymbol{x}$, $\mathcal{V} \to \boldsymbol{v}$, $\mathcal{L} \to l$, $\mathcal{W} \to w$.

A. Motion outside the singularity neighborhood

The reference joint acceleration can be derived via (9) as:

$$\ddot{\boldsymbol{q}}^r = \boldsymbol{J}_e^+ \left(\dot{\boldsymbol{v}}_e^r - \dot{\boldsymbol{J}}_e \dot{\boldsymbol{q}} - \dot{\boldsymbol{v}}_b \right) + \beta \boldsymbol{n}, \tag{13}$$

where $\boldsymbol{v}_e = [v_{ex}\, v_{ey}]^T$ and $\boldsymbol{v}_b = [v_{bx}\, 0]^T$ denote the end-tip and base velocity vectors, respectively, $\boldsymbol{n}(\boldsymbol{q}, w_m^r)$ is a vector from the kernel of the manipulator Jacobian. β is an arbitrary scalar. For best vibration suppression performance (outside the singularity neighborhood) it should be determined as $\beta = 1/\det \boldsymbol{A}$, where $\boldsymbol{A} = \begin{bmatrix} \boldsymbol{J}_e^T & \boldsymbol{h}_{bm}^T \end{bmatrix}^T$ [21]. Upon entering the neighborhood, vibration suppression is switched off by setting $\beta = 0$. The reference end-tip velocity is:

$$\dot{\boldsymbol{v}}_e^r = \dot{\boldsymbol{v}}_e^d + \boldsymbol{K}_d(\boldsymbol{v}_e^d - \boldsymbol{v}_e) + \boldsymbol{K}_p(\boldsymbol{x}_e^d - \boldsymbol{x}_e). \tag{14}$$

$\boldsymbol{K}_d = \text{diag}\begin{bmatrix} k_{d1} & k_{d2} \end{bmatrix}$ and $\boldsymbol{K}_p = \text{diag}\begin{bmatrix} k_{p1} & k_{p2} \end{bmatrix}$ are feedback gain matrices. $\boldsymbol{x}_e^d = \boldsymbol{x}_e^d(s)$ denotes desired end-tip position, whereby $s = s(t)$ stands for a suitably chosen path parameter. $\boldsymbol{x}_e = [x_{ex}\, x_{ey}]^T$ is the end-tip position determined via direct kinematics relations from joint angle data. With this notation, we can ensure *trajectory reparameterization* upon entering the singularity neighborhood, as will be explained in the next subsection.

[1]Henceforth, a constant value will be denoted via an overbar.

The reference force $w_m^r = g_b v_{bx}$ that restricts the null vector $\boldsymbol{n}$, imposes the vibration suppression constraint on the flexible base, g_b denoting the desired additional damping. The base speed v_{bx} is measured by a suitable sensor (e.g. derived from a strain gauge signal).

B. Motion within the singularity neighborhood

Upon entering the neighborhood of a dynamic singularity, the vibration suppression capability deteriorates. The reason is, as already explained, that the CoM motion is unilaterally constrained due to the specific manipulator configuration (Fig. 2 (b)). Momentum conservation can be achieved in the unconstrained direction, when the CoM moves with a constant-speed component $\bar{v}_{cx}$ (Fig. 2 (c)). We should note that the CoM motion in the x direction and the imposed base force are related as follows:

$$w_m/m_{tot} = \dot{v}_{cx} = \boldsymbol{J}_{cx}\ddot{\boldsymbol{q}} + \dot{\boldsymbol{J}}_{cx}\dot{\boldsymbol{q}}, \tag{15}$$

where $\boldsymbol{J}_{cx} = \boldsymbol{h}_{bm}/m_{tot}$ stands for the CoM Jacobian along the x-axis. Hence, a constant momentum can be represented as

$$\bar{l}_b = m_{tot}\bar{v}_{cx}. \tag{16}$$

It should be apparent, though, that end-tip trajectory tracking and momentum conservation can not be both achieved simultaneously within the neighborhood because at the singularity one system DOF will be lost. To alleviate this problem, we propose a trajectory reparameterization approach. Thereby, it will be ensured that the end-tip tracks the desired path; the tracking speed, however, will be determined via the momentum conservation subtask. Taking into account (15), the accelerations of interest can be grouped as:

$$\begin{bmatrix} \dot{v}_{ey} \\ \dot{v}_{cx} \end{bmatrix} = \boldsymbol{J}\ddot{\boldsymbol{q}} + \dot{\boldsymbol{J}}\dot{\boldsymbol{q}}, \tag{17}$$

where $\boldsymbol{J} = \begin{bmatrix} \boldsymbol{J}_{ey} & \boldsymbol{J}_{cx} \end{bmatrix}^T \in \Re^{2\times 3}$ is a Jacobian matrix with partial derivatives for the end-tip and the CoM velocities. Then, the reference joint acceleration can be determined as:

$$\ddot{\boldsymbol{q}}^r = \boldsymbol{J}^+ \left(\begin{bmatrix} \dot{v}_{ey}^r \\ \dot{v}_{cx}^r \end{bmatrix} - \dot{\boldsymbol{J}}\dot{\boldsymbol{q}} \right) + \boldsymbol{n}_J, \tag{18}$$

$\boldsymbol{n}_J$ denoting a vector from the kernel of matrix $\boldsymbol{J}$. This vector is not used, though, since it will disappear at the singularity.

The reference CoM acceleration for momentum conservation can be written with the help of (11) and (16) as:

$$\dot{v}_{cx}^r = K_m(\bar{v}_{cx}^d - v_{cx}),$$

where $\bar{v}_{cx}^d = v_{cx}(t_{in})$, and the current CoM speed v_{cx} is determined via direct kinematics relations from joint angle data. The reference value for the end-tip motion, on the other hand, can be written as:

$$\dot{v}_{ey}^r = \dot{v}_{ey}^d + K_d(v_{ey}^d - v_{ey}) + K_p(x_{ey}^d - x_{ey}).$$

Note, however, that this control law is subjected to reparameterization via the relation $s = s(x_{ex}(t))$.

TABLE I

THE MODEL PARAMETERS.

m_b	0.4 kg	l_1	0.1 m
m_1	0.025 kg	l_2	0.1 m
m_2	0.285 kg	l_3	0.1 m
m_3	0.025 kg	l_{g1}	0.05 m
m_4	0.285 kg	l_{g2}	0.05 m
m_5	0.025 kg	l_{g3}	0.05 m
m_6	0.095 kg	I_1	0.0135 kgm^2
k_b	191 N/m	I_2	0.0135 kgm^2
d_b	0.33 Ns/m	I_3	0.00307 kgm^2

Note: I_1, I_2 and I_3 are given w.r.t. the joint centers.

C. Simulation results

The model parameters of the 3R planar flexible-base manipulator are given in Table I. The initial configuration is $\boldsymbol{q} = \begin{bmatrix} 0.0 & 20.0 & 20.0 \end{bmatrix}^T$ deg. The desired path is a straight-line parallel to the x axis, heading in the negative direction. Initially, the desired end-tip trajectory $(\boldsymbol{x}_e^d, \boldsymbol{v}_e^d, \dot{\boldsymbol{v}}_e^d)$ is determined by selecting $s(t)$ as a fifth-order spline function with zero initial and final conditions and with final time to be decided in each simulation. The feedback gains are set as: $\boldsymbol{K}_d = \text{diag}\begin{bmatrix} 2.0 & 2.0 \end{bmatrix} \times 10^2$ s^{-1}, $\boldsymbol{K}_p = \text{diag}\begin{bmatrix} 2.0 & 2.0 \end{bmatrix} \times 10^4$ s^{-2} and $k_m = 2.0 \times 10^2$ s^{-1}. The joint viscous damping coefficients are set as $\boldsymbol{D}_m = \text{diag}\begin{bmatrix} 0.05 & 0.05 & 0.05 \end{bmatrix}^{\text{T}}$ Nms/rad, while the injected additional base viscous damping is $g_b = 10$ Ns/m. The dynamic singularity neighborhood is determined via $a_{max} = 0.2$ m/s^2 and $d_{max} = 1.5 \times 10^3$ kg^{-1}m^{-3}. It should be noted that especially the entering of the neighborhood should be designed with some care. We found out that the determinant curve does not provide sufficient information to distinguish the neighborhood. On the contrary, the base acceleration threshold can be chosen in such a way that base acceleration due to the singularity can be clearly distinguished from base acceleration due to motion initialization/termination and/or due to vibration suppression. Further on, upon entering the dynamic singularity neighborhood, the trajectory is reparameterized as explained above. When leaving the neighborhood, the trajectory is once more reparameterized for smoothness with the respective nonzero state at t_{out} and the stationary final state.

We performed four simulations. In the first two simulations, the final time for the spline was set to 9 s, resulting in path tracking with a relatively low-speed. The results from these two simulations are shown in Figs. 3 and 4. In these figures, (a) displays the CoM speed along the x axis (upper plot) and the base deflection (lower plot); (b) shows the determinant $\det \boldsymbol{A}$ (upper plot) and β (lower plot). From Fig. 3 it is seen that initially, there was almost no base deflection. This is because the desired acceleration is relatively small, and also, because of the vibration suppression capability. Later, the base started to vibrate, though, which is obviously due to the dynamic singularity. Note that we did not switch off vibration suppression in the singularity neighborhood, hence $\beta = 1/\det \boldsymbol{A}$ became quite large. Note also that the singularity was not crossed because the determinant didn't change sign. After leaving the neighborhood, the vibrations were effectively suppressed.

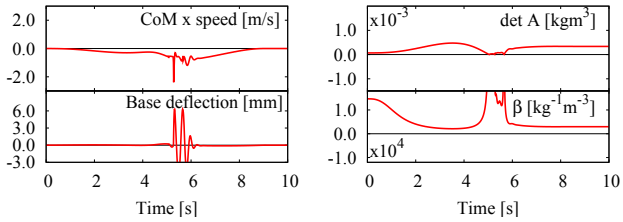

Fig. 3. Low-speed path tracking without switching off vibration suppression around the singularity. Significant base vibrations are induced. The singularity could not be crossed.

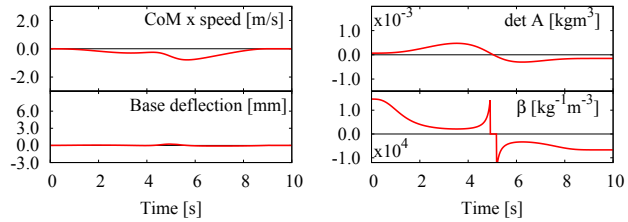

Fig. 4. Low-speed path tracking without vibration suppression around the singularity. The base deflects insignificantly. The singularity could be crossed.

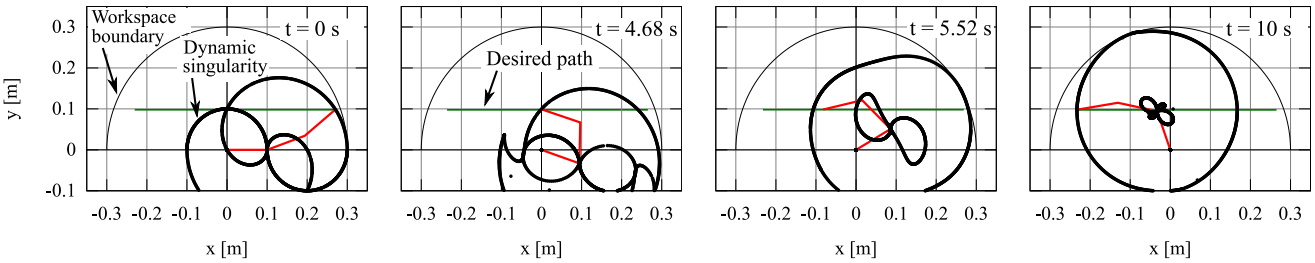

Fig. 5. Snapshots showing the variation of the dynamic singularities loci during path tracking with a relatively low speed. The curves are parameterized by the first joint angle and are centered, therefore, at the second joint. The green line is the desired path. The second snapshot ($t = 4.68$ s) shows the state just before entering the singularity neighborhood.

The results in Fig. 4, on the other hand, show that it is possible to move through the same singularity without any base disturbance. In this simulation, we simply switched off vibration suppression by setting $\beta = 0$ within the singularity neighborhood. The base was not disturbed significantly while crossing the singularity because the CoM didn't accelerate too much [21]. Fig. 5 shows the variation of the dynamic singularity curves (displayed in workspace) during straight-line path tracking. These curves are parameterized by the first joint angle, therefore they are centered at the second joint. It is seen that with the exception of the third snapshot ($t = 5.52$ s), the end-tip is always quite close to a singularity curve.

In the next two simulations, both the tracking speed and the acceleration were increased by shortening the final time for the spline function to 3.5 s. The respective results are shown in Figs. 6 and 7. The (a) and (b) data plots have the same meaning as those in the previous simulations. Additional data plots are included as follows: (c) and (d) are plots of the joint speeds and torques, respectively; (e) displays the end-tip tracking error in the y direction (upper plot) and the end-tip speed along x (lower plot). We should note that, in the third and fourth simulations, the vibration suppression control is switched off ($\beta = 0$) around the specified dynamic singularity.

Figure 6 shows results from a simulation without momentum conservation around the singularity. When compared to the last simulation (in Fig. 4), it is seen that the base deflected significantly upon entering the singularity neighborhood. There is no vibration, though, as in Fig. 3, because vibration suppression was switched off. The reason for base deflection is the disturbance due to a significant CoM acceleration, as can be seen from the upper plot in Fig. 6 (a). This disturbance, in combination with vibration suppression switching, is the reason why the joint speeds and torques are non-smooth, as seen from the (c) and (d) plots.

In the final simulation, we invoked momentum conservation upon entering the neighborhood, instead of only switching off vibration suppression. From the data plots in Fig. 7 (a) it is seen that the base deflection is considerably less than in the previous simulation. The reason is minimized base disturbance due to the almost constant CoM acceleration. Comparing the (c) and (d) plots in Figs. 6 and 7, we can conclude that motion in joint space is smoother in the latter simulation. The plot in Fig. 7 (e) shows that the end-tip speed profile was modified by the trajectory reparemeterization to accommodate the momentum conservation constraint.

V. CONCLUSIONS

We have shown that with a flexible-base manipulator, relatively high-speed path tracking through dynamic singularities is feasible, without inducing thereby significant base disturbance. This was made possible by conserving momentum upon entering the neighborhood of the singularity. We think that clarifying the above possibility is an important contribution to path planning and motion control of the subclass of flexible-base robots under consideration. It should be noted, though, that the method is path-dependent. Path reparameterization was proposed here to alleviate a problem related to loss of a DOF within the neighborhood of the singularity. But this approach may not succeed for any path, therefore, necessary conditions should be devised in a future work. Other issues, such as model uncertainty and robustness have to be considered as well. This we plan to do in a forthcoming study.

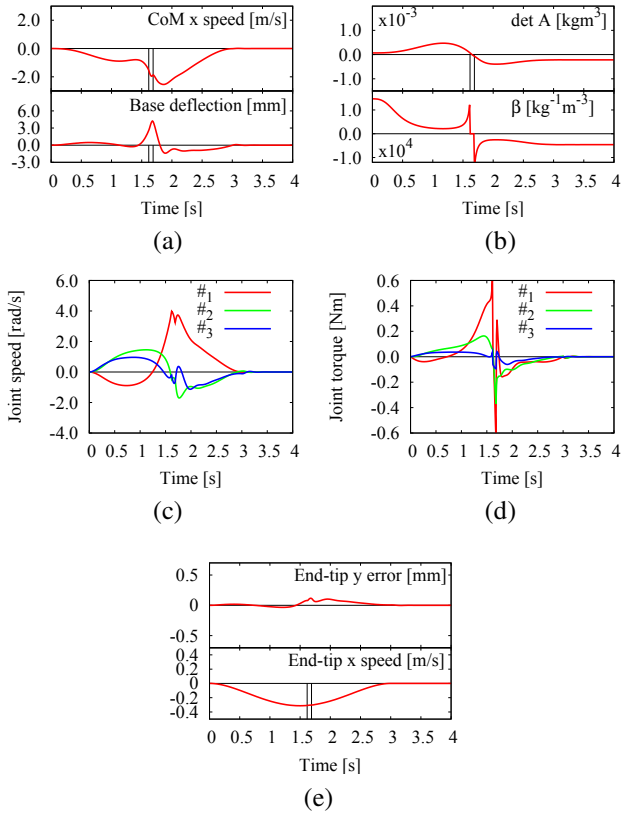

Fig. 6. High-speed path tracking without vibration suppression and momentum conservation around the singularity. The base deflects significantly due to the large acceleration of the CoM.

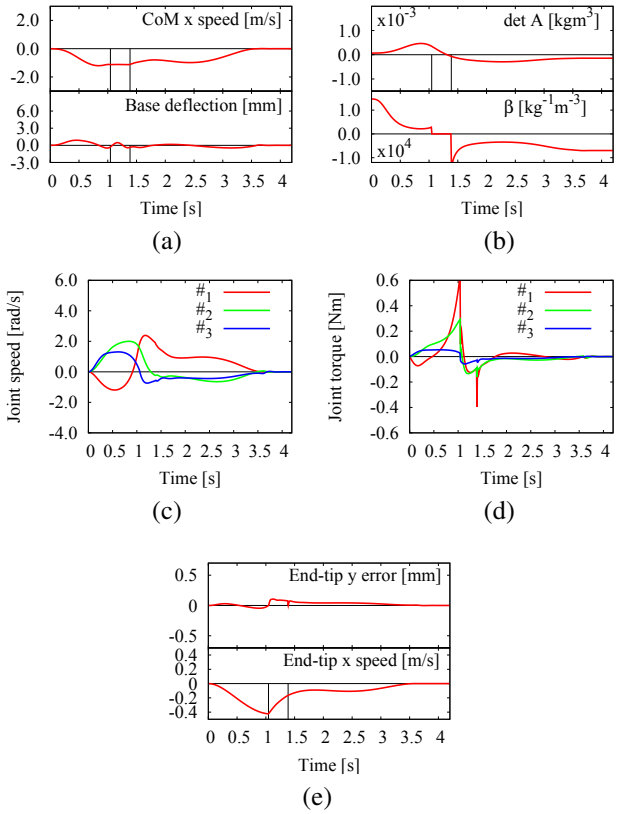

Fig. 7. High-speed path tracking without vibration suppression but with momentum conservation around the singularity. Trajectory reparameterization was invoked to ensure motion continuity, resulting in overall insignificant base deflection.

REFERENCES

[1] J. F. Jansen *et. al*, "Long-reach manipulation for waste storage tank remediation," in *Proc. of the ASME Winter Annual Meeting*, Atlanta, GA, USA, pp. 67–73, 1991.

[2] D. S. Kwon *et. al*, "Input shaping filter methods for the control of structurally flexible, long-reach manipulators," in *Proc. IEEE Int. Conf. Robot. Automat.*, San Diego, CA, USA, pp. 3259–3264, 1994.

[3] M. A. Torres and S. Dubowsky, "Path-planning in elastically constrained space manipulator systems," in *Proc. IEEE Int. Conf. Robot. Automat.*, Atlanta, GA, USA, pp. 812–817, 1993.

[4] C. Vallancourt and C. M. Gosselin, "Compensating for the structural flexibility of the SSRMS with the SPDM," in *Proc. 2nd Workshop Robot. Space, Canadian Space Agency*, Montreal, PQ, Canada, 1994.

[5] J. Ueda and T. Yoshikawa, "Robust arm configuration of manipulator mounted on flexible base," *IEEE Trans. on Robotics*, vol. 20, no. 4, pp. 781–789, Aug. 2004.

[6] J. Ueda *et. al*, "Solution of human-like redundant manipulator mounted on flexible body for task-space feedback control", in *Proc. ASME/IEEE Int. Conf. Adv. Intell. Mechatronics*, pp. 1429–1434, 2003.

[7] T. Wimböck *et. al*, "Experimental study on dynamic reactionless motions with DLR's humanoid robot Justin," in *Proc. 2009 IEEE/RSJ Int. Conf. on Intelligent Robots and Systems*, St. Louis, USA, Oct. 12–15, 2009.

[8] S. H. Lee and W. J. Book, "Robot vibration control using inertial damping forces," in *Proc. 8th CISM.–IFToMM Symp. RoManSy 8*, Cracow, Poland, pp. 252–259, Jul. 1990.

[9] M. A. Torres *et. al*, "Vibration control of deployment structures' long-reach manipulators: the P-PED method," in *Proc. 1996 IEEE Int. Conf. Robot. Automat.*, Minneapolis, MN, USA, pp. 2498–2504, Apr. 1996.

[10] Y. J. Lew and D. J. Trudnowski, "Vibration control of a micro/macro manipulator system," *IEEE Control Systems Magazine*, vol. 16, no. 1, pp. 26–31, Feb. 1996.

[11] I. Sharf, "Active damping of a large flexible manipulator with a short reach robot," *Trans. ASME, J. Dyn. Syst., Meas. Contr.*, vol. 118, no. 4, pp. 704–713, Dec. 1996.

[12] S. Abiko and K. Yoshida, "An adaptive control of a space manipulator for vibration suppression" in *Proc. 2005 IEEE/RSJ Int. Conf. on Intelligent Robots and Systems*, Edmonton, Canada, pp. 2167–2172, Aug. 2005.

[13] D. W. Cannon *et. al*, "Experimental study on micro/macro manipulator vibration control," in *Proc. IEEE Int. Conf. Robot. Automat.* , Minneapolis, Minnesota, pp. 2549–2554, Apr. 1996.

[14] R. H. Cannon, Jr. and E. Schmitz, "Initial experiments on the end-point control of a flexible one-link robot," *Int. J. Rob. Res.*, vol. 3, no. 3, pp. 62–75, 1984.

[15] C. Mavroidis *et. al*, "End-point control of long reach manipulator systems," in *Proc. 9th World Congr. IFToMM*, Milano, Italy, pp. 1740–1744, Sep. 1995.

[16] D. N. Nenchev *et. al*, "Reaction null-space control of flexible structure mounted manipulator systems," *IEEE Trans. on Robotics and Automation*, vol. 15, no. 6, pp. 1011–1023, Dec. 1999.

[17] D. N. Nenchev *et. al*, "Introduction of redundant arms for manipulation in space," in *IEEE Int. Workshop on Intelligent Robots and Systems*, Tokyo, Japan, 1988, pp. 679–684.

[18] Y. Fukazu *et. al*, "Pseudoinverse-based motion control of a redundant manipulator on a flexible base with vibration suppression," *J. of Robotics and Mechatoronics*, vol. 20, no. 4, pp. 621–627, 2008.

[19] Y. Fukazu *et. al*, "Reactionless resolved acceleration control with vibration suppression capability for JEMRMS/SFA," *Robotics and Biomimetics*, Bangkok, Thailand, pp. 1359–1364, Feb. 2009.

[20] E. Papadopoulos and S. Dubowsky, "Dynamic singularities in free-floating space manipulators," in *contributed chapter in Space Robotics: Dynamics and Control*, Y. Xu and T. Kanade, Eds. Boston, MA, USA: Kluwer Academic Publishers, 1993, pp. 77–100.

[21] N. Hara *et. al*, "Singularity-consistent torque control of a redundant flexible-base manipulator," in *Motion and Vibration Control*, Dordrecht, Netherlands, Springer Netherlands, pp. 103–112, Dec. 2008.